PCCP

PAPER

View Article Online
View Journal | View Issue

Cite this: *Phys. Chem. Chem. Phys.*, 2014, **16**, 14015

Substituted diphenyl butadiynes: a computational study of geometries and electronic transitions using DFT/TD-DFT†

Avik Kumar Pati,[a] Santosh J. Gharpure*[ab] and Ashok K. Mishra*[a]

Received 8th February 2014,
Accepted 21st May 2014

DOI: 10.1039/c4cp00580e

www.rsc.org/pccp

This work is aimed at theoretical understanding of electronic absorption and emission energies of a series of substituted diphenyl butadiynes through an assessment of several TDDFT functionals and a detailed study of solvent effects on their ground and excited state structures and properties. Out of a series of functionals examined, the coulomb attenuated DFT functional CAM-B3LYP is found to be most successful in predicting charge transfer absorption and emission energies of such derivatives. However, TDDFT potential energy surfaces obtained from hybrid functionals such as B3LYP and PBE0 are found to give a good description of the stability of locally excited (LE) and intramolecular charge transfer (ICT) states as a function of torsional angle, for the butadiynyl fluorophores. Interesting structural variations are observed in the ground and excited state optimized geometries of the fluorophores. The ICT emission of the butadiynyl fluorophores is observed to originate from the twisted state where the two phenyl rings in the diphenyl butadiyne get twisted around the butadiyne moiety. A bending of the butadiyne moiety is noted for some of the butadiynyl derivatives in the ICT emissive state. In addition, the direction of absorption and emission transition dipole moment vectors of the butadiynyl fluorophores is found to depend on the nature of substituents present at the periphery of the diphenyl butadiyne moiety.

Introduction

Diphenyl butadiynes have emerged as one of the important candidates among alkynyl derivatives in both experimental and theoretical research. While the butadiynyl derivatives have found applications in liquid crystals,[1–4] molecular rotors,[5] supramolecular stabilization[6] and anti-viral properties;[7] their structural, vibrational and electronic properties[8–14] have also gained considerable interest. The butadiynyl derivatives are also found to be effective fluorescent probes leading to the development of fluorescent anion sensors.[15] The diphenyl butadiynyl derivatives being the simplest butadiynyl chromophores often enjoy the credit of modern research pertaining to diyne derivatives in different spectroscopic fields. Recently, we also studied the photophysical properties of the butadiyne moiety in the substituted diphenyl butadiynes.[16] However, spectroscopic studies on the excited state of the diphenyl butadiynyl derivatives are deficient in the literature. An extensive understanding of geometries of electronically excited states of the butadiynes and related properties would shed light on the understanding of molecular dynamics of such derivatives. Ma *et al.* have described the absorption spectra and intramolecular charge transfer character of donor–acceptor substituted α,ω-diphenyl polyynes in their recent theoretical investigations.[17] Ikoma and Nagano *et al.* have explained the excited state symmetry switching of α,ω-diphenyl polyynes.[18] All the reported theoretical studies have focused on the understanding of optoelectronic properties of polyynes with the varying number of alkyne units where an exclusive theoretical study of a single class of fluorophores containing a definite number of alkyne units is lacking. Thus, a detailed and systematic theoretical understanding of both ground and excited states of the promising alkyne based fluorophoric family having two alkyne units—diphenyl butadiynyl derivatives—is highly desirable. While the reported studies on the polyyne system have mainly stressed upon neutral and donor–acceptor derivatives, a thorough theoretical investigation of diversely substituted diphenyl butadiynes such as donor–donor, donor–neutral, and neutral–acceptor derivatives is also desired for the present.

Density functional theory (DFT) has been the widely used theoretical approach among computational chemists in recent years. The successful journey of DFT in computational chemistry dates back when Becke introduced the hybrid functional B3LYP

[a] *Department of Chemistry, Indian Institute of Technology Madras, Chennai 600036, Tamil Nadu, India. E-mail: mishra@iitm.ac.in; Fax: +91-44-22574202; Tel: +91-44-22574207*

[b] *Department of Chemistry, Indian Institute of Technology Bombay, Powai, Mumbai 400076, India. E-mail: sjgharpure@iitb.ac.in; Fax: +91-22-2576-7152; Tel: +91-22-2576-7171*

† Electronic supplementary information (ESI) available: Figures and tables which are not provided in the main text. See DOI: 10.1039/c4cp00580e

in the literature.[19,20] The hybrid DFT functionals which include the exchange functional as a linear combination of HF exchange and DFT exchange have wider applications in transition state and excitation energy calculations than conventional pure DFT functionals.[21–23] The time dependent extension of DFT, namely TDDFT, has also received a wider acclaim for the excitation energy calculations of electronically excited states.[24–28] Although TDDFT enjoys huge success, it carries its drawbacks as it underestimates long-range charge transfer excitation energies.[29–36] To circumvent the problem of underestimation of long-range charge transfer excitation energy, long-range exchange corrections (LC) have been invoked in DFT functionals where the exact exchange–correlation (xc) is substituted by the admixture of position dependent HF exchange and DFT exchange–correlation,[33,37–49] which is in contrast to the conventional hybrid functional containing a constant fraction of HF exchange. Savin and co-workers[38,41] and Gill[37] *et al.* put forward a long-range correction scheme where the electron repulsion operator $1/r_{12}$ is divided into two parts—one is short range and another one is the long range part which are described using standard error function. Tawada *et al.* applied long-range correction for exchange functionals, reproducing the correct asymptotic potential energy behavior for the ethylene–tetrafluoroethylene derivative.[33] Long-range corrections for generalized gradient approximation (GGA) functionals with HF exchange using standard error function were introduced by Iikura *et al.*[39] The short-range exchange interaction was expressed through the pure density functional and the long-range exchange interaction was described through HF exchange in the long-range corrections. Yanai and Peach *et al.*[42,45,47] presented the coulomb attenuated hybrid exchange–correlation functional (CAM-B3LYP) implementing different proportions of HF exchange for different ranges of space. Scuseria and co-workers[49–52] produced several long-range corrected functionals and examined such functionals in excitation energy calculations of different molecular systems. The applicability of the CAM-B3LYP functional was extensively checked by Peach *et al.*[53]

In this article, we investigate the performance of several TDDFT functionals in the calculation of charge transfer absorption and emission energies of a series of substituted diphenyl butadiynes. Furthermore, we thoroughly investigate the effect of solvent contributions to the ground and excited state structures and properties of the butadiynyl derivatives to understand the charge transfer behavior of such derivatives. Next, a study of the transition dipole moment (TDM) vector of the butadiynyl fluorophores is carried out to understand the effect of substituents on TDM.

Computational details

All calculations were carried out using the Gaussian 09 computational suite.[54] Ten functionals such as BLYP,[55,56] PBE,[57] B3LYP,[20] PBE0,[58,59] M06-2X,[23] M05-2X,[60] LC-BLYP,[33] LC-PBE,[39,61] B98,[62] and CAM-B3LYP[42] were used for TDDFT vertical electronic absorption calculations. The ground state geometry optimized with the B3LYP method at the 6-311G(d,p) level of theory was considered for TDDFT absorption calculations. Various basis sets were screened in ground state geometry optimization calculation of the fluorophore **PhPh** and all the basis sets gave almost similar results. Thus, the ground state geometry of all the fluorophores was optimized using the 6-311G(d,p) basis set without the usage of diffuse function and thereby reducing computational cost. The frequency calculations were performed at the optimized geometry using B3LYP/6-311G(d,p) level of theory to ascertain whether the optimized geometry is at the stationary point without any imaginary frequency.

The locally excited (LE) state and intramolecular charge transfer (ICT) state geometries were optimized by TD-B3LYP/6-311G(d,p) level of theory with C_1 symmetry and the minima were confirmed through frequency calculations. The excited state optimized geometry was employed to compute emission energies as vertical de-excitations using the TDDFT method with B3LYP, PBE0, M052X, LC-BLYP, and CAM-B3LYP functionals. The effect of solvent in the absorption and emission energy calculations was studied through the self-consistent reaction field (SCRF) using the polarizable continuum model (PCM)[63] which considers a cavity inside the solvent, and a solute molecule is entrapped inside the cavity distributing its charge on the surface of the cavity, outside of which is regarded as a continuum mainly characterized by the dielectric constant. It is pertinent to mention that the standard parameters ($\alpha = 0.19$, $\beta = 0.46$, and $\mu = 0.33$) were used for the CAM-B3LYP functional. For the long range corrected functional LC-BLYP, the standard μ value ($\mu = 0.33$) was used for all the calculations. The TD-CAM-B3LYP functional was also used to optimize the charge transfer excited state so as to compare the geometry with the TD-B3LYP optimized geometry.

Results and discussion

Effect of solvent on the ground state geometry

The gas phase optimized ground state geometries of the fluorophores under study here are represented in Fig. 1. Cyclohexane, heptane, dioxane, tetrahydrofuran (THF), dichloromethane (DCM), isopropanol, methanol (MeOH), acetonitrile (CH_3CN), and *N*,*N*-dimethylformamide (DMF) were chosen as solvents of choice in our investigation. The ground state optimized structures of all the fluorophores but **Me_2NMe_2N** were found to be almost planar not only in the gas phase (Fig. 1) but also in solvents of varying polarities (see Fig. S1, ESI†). The ground state geometry of the fluorophore **Me_2NMe_2N** was observed to be particularly interesting given the fact that it is planar in the gas phase, partially twisted in non-polar to moderately polar solvents like cyclohexane, heptane, dioxane, THF, DCM, isopropanol and MeOH, and almost completely twisted in highly polar solvents like CH_3CN and DMF (Fig. 2). The observed twisting is not the twist of the C(Ph)–N(NMe_2) bond which is very common in dimethyl amino substituted fluorophores in photochemistry, rather it is the twist of two phenyl rings around the butadiyne moiety. As solvent polarity increases, the partially twisted molecule gets converted

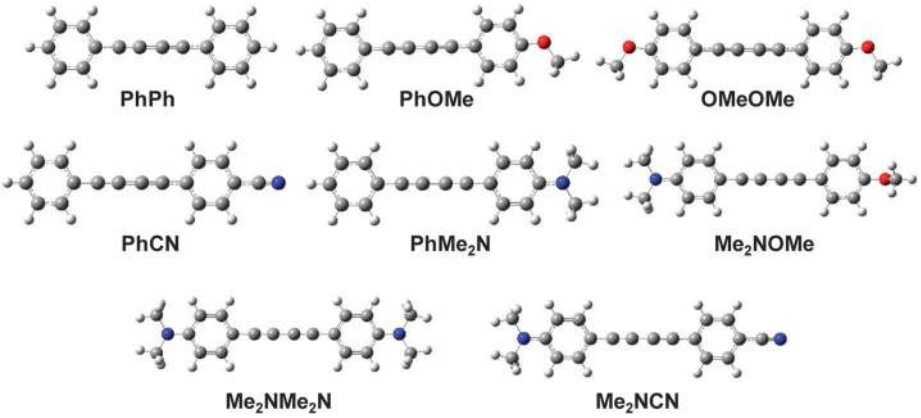

Fig. 1 Ground state optimized geometry of the butadiynyl fluorophores in the gas phase at B3LYP/6-311G(d,p) level of theory.

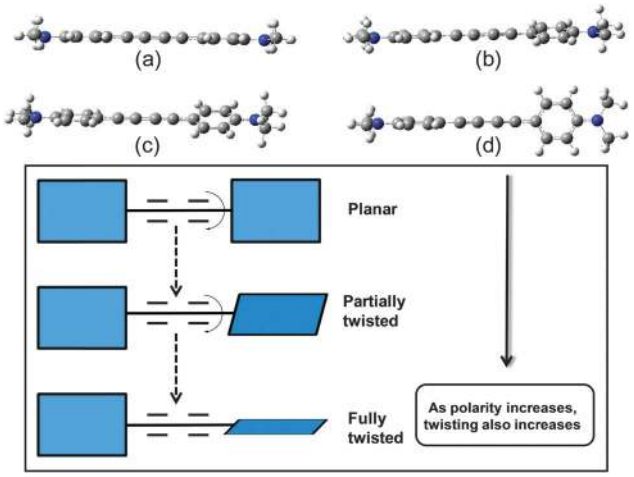

Fig. 2 Ground state optimized geometry of **Me_2NMe_2N** in (a) gas phase, (b) cyclohexane, (c) DCM, and (d) CH_3CN using B3LYP/6-311G(d,p) (cartoon diagram is inside the box).

into the almost fully twisted derivative. The observed twisting of the phenyl rings around the diacetylenic moiety in **Me_2NMe_2N** with increasing solvent polarity could be attributed to the combined effect of charge transfer and substituent effects. It was found that Mulliken charge on the second acetylenic carbon of the butadiyne moiety in **Me_2NMe_2N** which is +0.167 in the gas phase, decreases with increasing solvent polarity (see Fig. S2, ESI†). The NMe_2 group was found to be almost co-planar with the attached phenyl ring for the fluorophores in the ground state.

The geometrical parameters like the twist angle of the NMe_2 group, the change in pyramidalization of the NMe_2 group, and the C(Ph)–N(NMe_2) bond length were studied for the derivatives containing the NMe_2 group such as **$PhMe_2N$**, **Me_2NOMe**, and **Me_2NCN** in the ground state with the variation of the dielectric constant. Fig. 3a and b show that both the twist angle and pyramidalization of the NMe_2 group decrease with increase in the polarity of the solvents. For the derivative **$PhMe_2N$**, the twist angle and pyramidalization gradually decrease from the gas phase to DCM (ε = 8.93), and then there is a slight increase up to DMF (ε = 37.219). Both the twist angle and pyramidalization of the NMe_2 group in **Me_2NOMe** almost steadily decrease up to DMF with a small discrepancy, where a slight increment of the angle has been found in cyclohexane (ε = 2.0165) and dioxane (ε = 2.2099). A sharp decrease of the twist angle and pyramidalization has been observed for **Me_2NCN** from the gas phase to dioxane and then almost constant up to MeOH (ε = 32.613) with a small increase in CH_3CN and DMF. The overall decrease of the twist angle as well as pyramidalization of the NMe_2 group with increasing solvent polarity indicates that the lone pair of electrons on the nitrogen atom of the NMe_2 group gets more delocalized on the extended π system upon increasing the polarity of solvents (see Fig. S3–S5 in ESI† for Mulliken charge analysis).

The change in the C(Ph)–N(NMe_2) bond length (Fig. 3c) is almost in accordance with the observations of the variation of twist angle and pyramidalization of the NMe_2 group with the dielectric constant. Fig. 3 demonstrates that the twist angle as well as the pyramidalization of the NMe_2 group, and the C(Ph)–N(NMe_2) bond length are highest for **Me_2NOMe**, then **$PhMe_2N$** and the lowest for **Me_2NCN**. This is attributed to the fact that the electron delocalization of the NMe_2 group is maximum for the fluorophore **Me_2NCN** because of the presence of a strong electron withdrawing group CN whereas it is least for **Me_2NOMe** which has a weak donor methoxy (OMe) group, and it is medium for **$PhMe_2N$** which has a neutral phenyl moiety (see Fig. S6 in ESI† for Mulliken charge analysis). The C(Ph)–O(OMe) bond length of the fluorophores containing the methoxy group **PhOMe**, **OMeOMe**, and **Me_2NOMe** was also observed to decrease (see Fig. S7, ESI†), similar to the decrease of the C(Ph)–N(NMe_2) bond length for the NMe_2 containing derivatives **$PhMe_2N$**, **Me_2NOMe**, and **Me_2NCN** with increase of solvent polarities (Fig. 3c). Thus, the observed data in the ground state geometry of the fluorophores are in support of possible charge transfer behavior. As expected, the C(Ph)–N(CN) bond length of the nitrile containing fluorophores **PhCN** and **Me_2NCN** increases with increasing dielectric constant of solvents (Fig. 4). The derivative **Me_2NCN** having a strong donor group NMe_2 pushes electrons through the butadiyne moiety much better than the derivative **PhCN** which has a neutral phenyl moiety as the donor group, thus lengthening the nitrile bond much higher than that in the **PhCN** derivative.

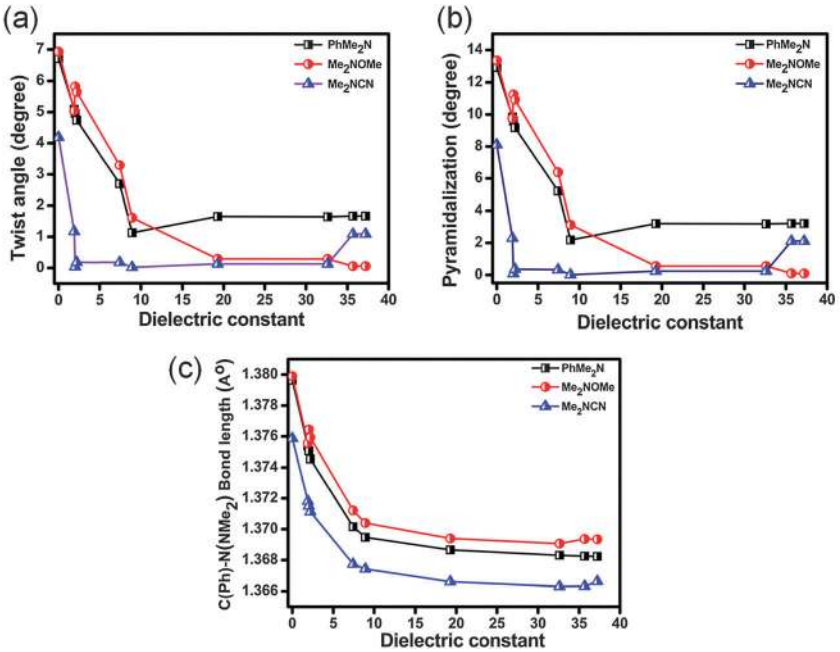

Fig. 3 Correlation of (a) twist angle, (b) pyramidalization, and (c) C(Ph)–N(NMe_2) bond length with dielectric constant at ground state B3LYP/6-311G(d,p) optimized geometry.

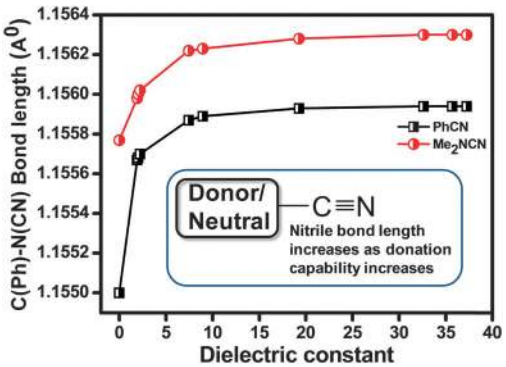

Fig. 4 Correlation of the C(Ph)–N(CN) bond length with the dielectric constant at ground state B3LYP/6-311G(d,p) optimized geometry.

TD-DFT assessment of functionals for vertical electronic absorption energy calculations

Insight into the understanding of electronic transitions of the fluorophores was embarked through TDDFT calculations of the ground state geometry of the fluorophores optimized at B3LYP/6-311G(d,p) level of theory. Exchange–correlation functionals like BLYP, and PBE; hybrid functionals such as B3LYP, B98, PBE0, M06-2X, and M05-2X, and long-range corrected functionals such as LC-BLYP, LC-PBE, and CAM-B3LYP were examined for evaluating absorption energies of the fluorophores (Tables 1 and 2). The experimental λ_{max} of absorption in Tables 1 and 2 indicates the lowest energy 0–0 absorption. It is important to mention here that it appeared a bit difficult to accurately determine the 0–0 absorption energy values from our earlier experimental absorption spectra[16] which were found to be of low resolution. Therefore, the absorption spectra of the butadiynyl fluorophores were recorded with high resolution in cyclohexane (see Fig. S8 and S9, ESI†) and the 0–0 absorption values thus obtained from the high resolution spectra were used here to compare the computational data with the experimental one in Tables 1 and 2. However, in the subsequent section of basis set study the absorption values of **Me_2NCN** in polar solvents were taken from our earlier spectra[16] because spectral resolution did not make much difference since the vibrational fine structures of the longest wavelength band of **Me_2NCN** were significantly lost in polar solvents. Although the theoretically computed absorption energy corresponds to vertical transition, it is still popular in understanding the absorption phenomenon compared with the experimental data. The exchange–correlation functionals BLYP and PBE highly underestimate charge transfer absorption energy of the butadiynyl fluorophores whereas the hybrid functionals B3LYP, B98, PBE0, M06-2X, and M05-2X perform much better than the exchange–correlation functionals (Tables 1 and 2). Among the hybrid functionals used in our study, the PBE0 functional was found to be effective in estimating charge transfer absorption energies of the butadiynyl fluorophores.[17] The hybrid functionals are generally found to perform better as the % of HF exchange increases (Fig. 5). On the other hand, the long-range correction of the exchange–correlation functionals improves the absorption energies compared to the pure exchange–correlation functionals (Table 2). The better performance of the long-range corrected DFT functionals could be attributed to the gradual addition of HF exchange with the increase of inter-electronic distance. Pleasingly, the coulomb-attenuated DFT functional CAM-B3LYP was found to be the most effective functional among the various functionals screened here in calculating the absorption energies of the

Table 1 Computed $S_0 \rightarrow S_1$ absorption wavelength (λ_{abs}), oscillator strength (f), and orbital transition at BLYP, PBE, B3LYP, B98 and PBE0 levels of theory in cyclohexane

Molecule	Exp λ_{abs} (nm)	BLYP/6-311G(d,p) λ_{abs} (nm)	f	Orbital transition	PBE/6-311G(d,p) λ_{abs} (nm)	f	Orbital transition	B3LYP/6-311G(d,p) λ_{abs} (nm)	f	Orbital transition	B98/6-311G(d,p) λ_{abs} (nm)	f	Orbital transition	PBE0/6-311G(d,p) λ_{abs} (nm)	f	Orbital transition
PhPh	328	378.21	1.1974	H[a] → L[b] H − 1 → L + 1	375.35	1.2171	H → L H − 1 → L + 1	349.75	1.1556	H → L H − 1 → L + 1	347.69	1.1526	H → L H − 1 → L + 1	341.29	1.676	H → L H − 1 → L + 1
OMeOMe	339	399.18	1.5385	H → L H − 2 → L + 3	396.89	1.6172	H → L H − 2 → L + 3	362.33	1.5049	H → L H − 2 → L + 3	359.64	1.5008	H → L H − 2 → L + 3	353.08	1.5243	H → L H − 2 → L + 3
Me_2NMe_2N	370	439.86	1.8038	H → L	439.70	1.8204	H → L	390.63	1.9038	H → L H − 2 → L + 1	387.22	1.9133	H → L H − 2 → L + 1	380.27	1.9501	H → L H − 2 → L + 1
PhCN	343	413.17	1.2816	H → L H − 1 → L + 3	410.36	1.2971	H → L H − 1 → L + 3	373.28	1.3574	H → L H − 1 → L + 3	370.39	1.3656	H → L H − 1 → L + 3	362.99	1.3855	H → L H − 1 → L + 3
PhOMe	336	395.83	1.3080	H → L H − 1 → L + 2	394.20	1.3172	H → L H − 1 → L + 2	359.21	1.3222	H → L H − 1 → L + 2	356.59	1.3218	H → L H − 1 → L + 1	350.01	1.3419	H → L H − 1 → L + 1
$PhMe_2N$	363	447.15	1.1609	H → L H → L + 4	383.77	1.4787	H → L H → L + 4	387.70	1.4569	H → L H − 2 → L + 1	383.77	1.4787	H → L H − 2 → L + 1	376.56	1.5104	H → L H − 2 → L + 1
Me_2NOMe	360	433.02	1.4592	H → L	432.70	1.4773	H → L H → L + 4	382.55	1.6755	H → L H − 2 → L + 2	379.09	1.6874	H → L H − 2 → L + 2	372.20	1.7194	H → L H − 2 → L + 2
Me_2NCN	399	537.26	1.0359	H → L H → L + 2	538.91	1.0351	H → L H → L + 2	443.72	1.3992	H → L	436.97	1.4456	H → L	427.05	1.4881	H → L

[a] H stands for HOMO. [b] L stands for LUMO.

Table 2 Computed $S_0 \rightarrow S_1$ absorption wavelength (λ_{abs}), oscillator strength (f), and orbital transition at M06-2X, MO5-2X, LC-BLYP, LC-PBE and CAM-B3LYP levels of theory in cyclohexane

Molecule	Exp λ_{abs} (nm)	M06-2X/6-311G(d,p) λ_{abs} (nm)	f	Orbital transition	M05-2X/6-311G(d,p) λ_{abs} (nm)	f	Orbital transition	LC-BLYP/6-311G(d,p) λ_{abs} (nm)	f	Orbital transition	LC-PBE/6-311G(d,p) λ_{abs} (nm)	f	Orbital transition	CAM-B3LYP/6-311G(d,p) λ_{abs} (nm)	f	Orbital transition
PhPh	328	315.44	1.1666	H[a] → L[b] H − 1 → L + 2	316.98	1.1553	H → L H − 1 → L + 1	303.21	0.8771	H → L H − 1 → L + 2 H → L + 7 H − 2 → L + 1	299.21	0.9221	H → L H − 1 → L + 2 H − 2 → L + 1 H → L + 7	323.47	1.0247	H → L H − 1 → L + 2
OMeOMe	339	324.56	1.5171	H → L H − 2 → L + 3	325.47	1.4955	H → L H − 2 → L + 1	309.79	1.1948	H → L H − 2 → L + 3 H − 5 → L H − 1 → L + 4	306.15	1.2577	H → L H − 2 → L + 3 H − 5 → L H − 1 → L + 4	331.69	1.3607	H → L H − 1 → L + 4 H − 2 → L + 3
Me_2NMe_2N	370	347.06	2.0231	H → L H − 1 → L + 4 H − 2 → L + 2	347.16	2.0079	H → L H − 1 → L + 4 H − 2 → L + 1	324.57	1.7017	H → L H − 1 → L + 4 H − 1 → L + 1 H − 2 → L + 1 H − 3 → L	321.76	1.7873	H → L H − 1 → L + 4 H − 1 → L + 1 H − 2 → L + 1 H − 3 → L	350.47	1.8451	H → L H − 1 → L + 4 H − 2 → L + 1 H − 3 → L
PhCN	343	330.93	1.4144	H → L H − 1 → L + 3	332.31	1.4100	H → L H − 1 → L + 3	313.61	1.1220	H → L H − 1 → L + 3 H − 3 → L + 1 H → L + 1 H → L + 7	309.70	1.1742	H → L H − 1 → L + 3 H − 3 → L + 1 H → L + 1 H → L + 5	338.02	1.2780	H → L H − 1 → L + 3
PhOMe	336	321.54	1.3476	H → L H − 1 → L + 2	322.65	1.3316	H → L H − 2 → L + 1	307.31	1.0453	H → L H − 2 → L + 4 H − 1 → L + 2 H − 1 → L	303.56	1.1007	H → L H − 2 → L + 3 H − 1 → L + 2 H − 1 → L	328.88	1.2014	H → L H − 2 → L + 2
$PhMe_2N$	363	340.84	1.6169	H → L H − 1 → L H − 2 → L + 1	341.04	1.6125	H → L H − 1 → L H − 2 → L + 1	318.99	1.3443	H → L H − 1 → L H − 2 → L + 4 H − 1 → L + 2 H → L + 2	315.97	1.4122	H → L H − 1 → L H − 1 → L + 2 H − 2 → L + 3	344.60	1.4789	H → L H → L + 4 H − 1 → L H − 2 → L + 1
Me_2NOMe	360	339.54	1.7825	H → L H − 2 → L + 2	339.83	1.7686	H → L H − 1 → L + 4 H − 1 → L H − 1 → L + 2	319.28	1.4732	H → L H − 1 → L + 4 H − 1 → L H − 2 → L + 3 H − 5 → L	316.21	1.5468	H → L H − 1 → L + 4 H − 1 → L H − 2 → L + 3 H − 5 → L	343.97	1.6245	H → L H − 1 → L + 4 H − 1 → L H − 2 → L + 2
Me_2NCN	399	371.19	1.7519	H → L H → L + 2 H − 1 → L H − 2 → L + 3	370.96	1.7717	H → L H → L + 1 H − 1 → L H − 2 → L + 3	336.46	1.5991	H → L H − 1 → L H → L + 1 H − 2 → L + 3	333.70	1.6640	H → L H − 1 → L H → L + 1 H − 2 → L + 3	371.87	1.6810	H → L H − 1 → L H − 2 → L + 3 H → L + 1

[a] H stands for HOMO. [b] L stands for LUMO.

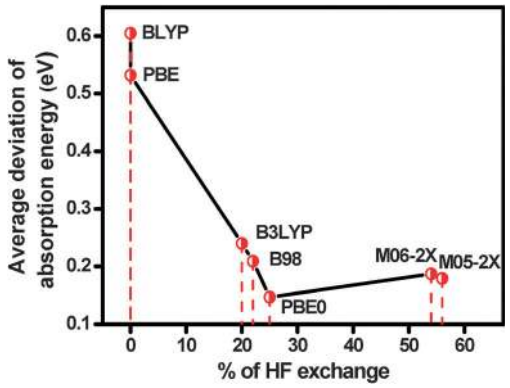

Fig. 5 Correlation of average deviation of absorption energy ($S_0 \rightarrow S_1$) from experimental values with % of HF exchange in cyclohexane.

butadiynyl fluorophores. Thus, the CAM-B3LYP functional establishes itself as an effective functional in the evaluation of long-range charge transfer absorption energies of the butadiynyl derivatives. It is observed that the average deviations of calculated absorption energy from the experimental values for the series of the butadiynyl derivatives discussed here are 0.605, 0.532 eV for BLYP, and PBE; 0.240, 0.209, 0.147, 0.187, 0.179 eV for B3LYP, B98, PBE0, M06-2X, and M05-2X; while 0.402, 0.452, 0.128 eV for LC-BLYP, LC-PBE, and CAM-B3LYP respectively in cyclohexane. Thus, the CAM-B3LYP functional was found to outperform all other functionals used in this study.

Screening of basis sets

Having optimized the choice of functional in determining absorption energies of the butadiynyl fluorophores, the effect of the basis set was carefully examined using the CAM-B3LYP functional (Table 3). The fluorophore **Me_2NCN** was considered as a test molecule for the basis set study. Split-valence basis sets such as 6-31G(d), 6-31+G(d), 6-311G(d,p), 6-311+G(d,p), and 6-311++G(d,p) were used here for the investigation. The basis set study was accompanied by the incorporation of solvent effect contribution through the PCM model[63] so as to compare the calculated wavelength values with the experimentally observed data[16] in solvents of different polarities. It is observed that the inclusion of diffusion function improves the calculated absorption wavelength value compared with the experimental one. The incorporation of one diffuse function in 6-311G(d,p) increases the absorption wavelength value by 2.88 nm whereas the addition of two diffuse functions increases the absorption wavelength value by 2.92 nm in cyclohexane. Since 6-311+G(d,p), and 6-311++G(d,p) basis sets gave almost closer values of absorption wavelengths, the 6-311+G(d,p) basis set was chosen for further studies compromising with accuracy and computational cost. From this point onward, CAM-B3LYP/6-311+G(d,p) level of theory will be discussed for TDDFT vertical electronic excitation energy calculations.

Effect of solvents on the vertical electronic absorptions and molecular orbitals

Intrigued by the finding of CAM-B3LYP/6-311+G(d,p) level of theory as an effective theoretical tool in the evaluation of charge transfer absorption energies of the butadiynyl fluorophores, a detailed study on the vertical absorption of the first three singlet excited states of the butadiynyl fluorophores was carried out in different solvents of varying polarities. The $S_0 \rightarrow S_1$ transition energy is found to get stabilized from gas phase to solvents for all the fluorophores (see Fig. S10 and S11, ESI†). But, the energy very soon reaches a saturation point at $\varepsilon = 8.93$ for DCM after which it does not change much with increasing solvent polarity. The $S_0 \rightarrow S_1$ absorption wavelength is slightly blue shifted from heptane to MeOH and then a slight red shift to CH_3CN and DMF. However, the solvatochromic shift of the $S_0 \rightarrow S_1$ absorption wavelength of the fluorophores is found to be negligible, which is in accordance with earlier experimental findings.[16] Interestingly, the $S_0 \rightarrow S_2$ transition energy gets destabilized from the gas phase to solvents for **PhPh**, **PhOMe**, and **PhCN** whereas destabilization of the $S_0 \rightarrow S_3$ transition energy is observed for **PhOMe**, **OMeOMe**, **PhMe$_2$N**, **Me$_2$NMe$_2$N**, and **Me$_2$NOMe** from the gas phase to solvents (see Fig. S10 and S11, ESI†).

The highest occupied molecular orbital (HOMO) and lowest unoccupied molecular orbital (LUMO) mainly contribute to the $S_0 \rightarrow S_1$ transition (see Tables S1 and S2, ESI†). The energy stabilization of the HOMO and LUMO of the butadiynyl fluorophores in different solvents is noteworthy (see Fig. S12, ESI†). In cyclohexane, it is noted that incorporation of one OMe group in **PhPh** increases the HOMO and LUMO energy in **PhOMe** by 0.011 and 0.006 a.u. respectively whereas addition of two OMe groups in **PhPh** increases the HOMO and LUMO energy in

Table 3 Screening of basis sets using the CAM-B3LYP functional for the fluorophore **Me_2NCN**

		Calculated $S_0 \rightarrow S_1$ λ_{abs} (in nm) using CAM-B3LYP/basis set				
Solvents	Exp[a,b] λ_{abs} (nm)	6-31G(d)	6-31+G(d)	6-311G(d,p)	6-311+G(d,p)	6-311++G(d,p)
Cyclohexane	399[b]	368.17	373.36	371.87	374.75	374.79
Dioxane	389[a]	368.52	373.76	372.25	375.15	375.19
THF	389[a]	371.65	377.23	375.60	378.64	378.68
DCM	390[a]	372.25	377.87	376.24	379.29	379.33
Isopropanol	385[a]	372.11	377.77	376.11	379.18	379.21
MeOH	383[a]	371.39	377.04	375.37	378.43	378.47
CH_3CN	385[a]	371.71	377.38	375.70	378.78	378.81
DMF	393[a]	373.33	379.07	377.41	380.50	380.53

[a] Ref. 16. [b] See ESI.

OMeOMe by 0.019 and 0.013 a.u. respectively. Similarly, the presence of one extra Me_2N group in **Me_2NMe_2N** compared to **$PhMe_2N$** increases the HOMO and LUMO energy of **Me_2NMe_2N** by 0.013 and 0.013 a.u. respectively. On the other hand, the presence of one extra weak donating OMe group in **Me_2NOMe** enhances its HOMO and LUMO energy by 0.005 and 0.007 a.u. respectively compared to **$PhMe_2N$**. The fluorophore **PhCN** having one strong electron withdrawing nitrile (CN) group helps to stabilize both its HOMO and LUMO by 0.011 and 0.021 a.u. compared with the neutral fluorophore **PhPh**. Similarly, the HOMO and LUMO of the fluorophore **Me_2NCN** which has the strong acceptor CN group, gets stabilized by 0.007 and 0.025 a.u. compared to **$PhMe_2N$**. Similar observations of orbital stabilization are also observed in other solvents of different polarities in addition to cyclohexane (see Fig. S12, ESI†).

TDDFT absorption energy of different rotamers

At this point, it is relevant to mention that the energy barrier to rotation of the phenyl rings around the diacetylene moiety is very low (order of 0.1 kcal mol^{-1}).[8] There has been a considerable amount of research to understand and analyze the absorption spectra of diphenyl butadiyne (**PhPh**) over the years.[8–14] Recently, Thulstrup *et al.*[8] emphasized on the possible contributions of different rotamers with planar geometry to the absorption spectra of diphenyl butadiyne (**PhPh**). Here, we have assigned the 0–0 absorption band to the planar geometry for the butadiynyl fluorophores. The complicated absorption spectra with strong vibronic progressions for the diversely substituted diphenyl butadiynyl derivatives[16] have restricted us from assigning all the absorption bands, anticipating the possible contributions of other rotamers to the other absorption bands, which are challenging and difficult to assign for the butadiynyl fluorophores. However, to shed light on the change in transition energy with different rotamers as well as to provide the information of very less energy barrier of rotation of the phenyl ring around the butadiyne moiety from one rotamer to another, the TDDFT potential energy surface (PES) with the twist angle of the phenyl ring around the diacetylene axis was studied for the butadiynyl fluorophores. It also suggested that the energy barrier to rotation of the phenyl rings is very low (order of 0.1 kcal mol^{-1}) and the transition energy is sensitive to the twist angle of the phenyl ring around the diacetylenic moiety of the fluorophores (Fig. 6 and see Fig. S13 and S14, ESI† for others). It is important to note that the PES obtained by using CAM-B3LYP functional shows almost barrier free transition between LE and ICT states for most of the butadiynyl fluorophores (Fig. S14, ESI†). Thus, it does not support our experimental observation[16] of the presence of the ICT state for the butadiynyl fluorophores. However, the TDDFT PES obtained using hybrid functionals such as B3LYP (Fig. 6) and PBE0 (Fig. S13, ESI†) gives the description of LE and ICT states for the butadiynyl fluorophores with distinct energy barrier. The B3LYP TDDFT PES (Fig. 6b) for **PhCN** exhibits a maximum at 45° while PBE0 TDDFT PES (Fig. S13b) for **PhCN** shows a maximum at 60°. The PES of donor–neutral **$PhMe_2N$** (Fig. 6a)

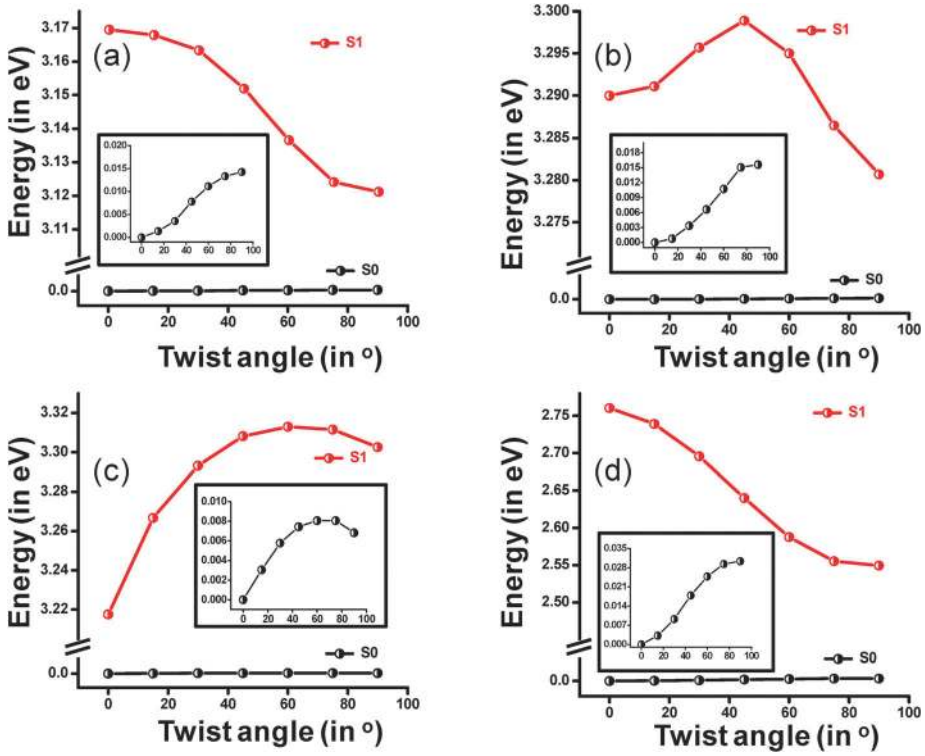

Fig. 6 TDDFT potential energy curves (energy relative to the minimum of the ground state) of the ground and 1st excited singlet state of (a) **$PhMe_2N$**, (b) **PhCN**, (c) **Me_2NOMe**, and (d) **Me_2NCN** in cyclohexane as a function of twist angle of the phenyl ring around the butadiyne moiety using B3LYP/6-311+G(d,p) (expanded energy scale of S_0 is in inset).

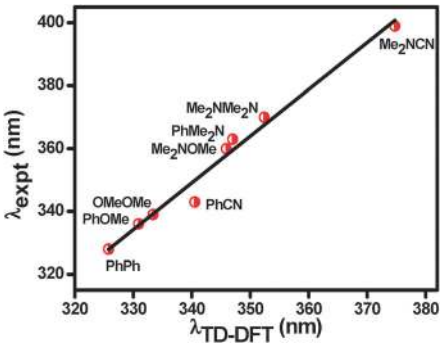

Fig. 7 Correlation between experimental and TD-DFT absorption wavelength in cyclohexane using CAM-B3LYP/6-311+G(d,p) level of theory.

and donor–acceptor **Me_2NCN** (Fig. 6d) shows a good stability of the ICT state whereas the PES of donor–donor **Me_2NOMe** (Fig. 6c) suggests greater stability of the LE state compared to the ICT state. Although the energy barrier is very less, it is noted that the donor–donor derivative **Me_2NOMe** exhibits slight stability of the twisted geometry even in the ground state.

Correlation between experimental and TD-DFT electronic absorption wavelengths

In the earlier section, we have discussed about the best predictive ability of CAM-B3LYP/6-311+G(d,p) level of theory in calculating charge transfer absorption energies of the butadiynyl fluorophores. We have mentioned that CAM-B3LYP/6-311G(d,p) level of theory produces the charge transfer absorption energy values of the fluorophores with an average error of 0.128 eV. However, a closer look at Table 2 reveals that the maximum deviation of calculated absorption energy from the experimental values using CAM-B3LYP occurs for the most prominent charge transfer active molecule **Me_2NCN**. In a deeper analysis, it is observed that the deviation actually starts increasing from dimethyl amino substituted fluorophores **Me_2NOMe** to **$PhMe_2N$** to **Me_2NMe_2N** to **Me_2NCN** where the deviations are found to be 0.14, 0.157, 0.167, and 0.201 eV respectively in cyclohexane considering CAM-B3LYP/6-311+G(d,p) absorption energy and the experimental values. At this juncture, we envisaged that a linear equation correlating experimental absorption wavelength and TD-DFT wavelength might help in improving the $\lambda_{TD\text{-}DFT}$ values of the highly charger transfer active molecule like **Me_2NCN**. As anticipated, a plot (Fig. 7) of λ_{expt} *vs.* $\lambda_{TD\text{-}DFT}$ produced a good linear fit with the R^2 value of 0.98, which has the form of

$$\lambda_{expt} = -156.77 + 1.49\lambda_{TD\text{-}DFT}$$

Pleasingly, the linear equation produced only 0.013, 0.026, 0.015, and 0.02 eV deviation of absorption energy from the experimental values for **Me_2NOMe**, **$PhMe_2N$**, **Me_2NMe_2N**, and **Me_2NCN** respectively. Thus, the empirical linear relationship helps to estimate more accurate charge transfer absorption energies of the butadiynyl fluorophores. The correlation between the experimental absorption wavelength and the TD-DFT absorption wavelength was also investigated in DCM, MeOH and CH_3CN producing a linear fit with good R^2 values (see Fig. S15–S17, ESI†).

Correlation between vertical excitation energy and solvent induced geometry change

Further, to understand the correlation of vertical excitation energy with ground state observed geometrical parameters such as the twist angle of the NMe_2 group, pyramidalization of the NMe_2 group, and the C(Ph)–N(NMe_2) bond length in different solvents, the NMe_2 containing derivative **$PhMe_2N$** has been chosen here as a representative (Fig. 8, see Fig. S18 and S19,

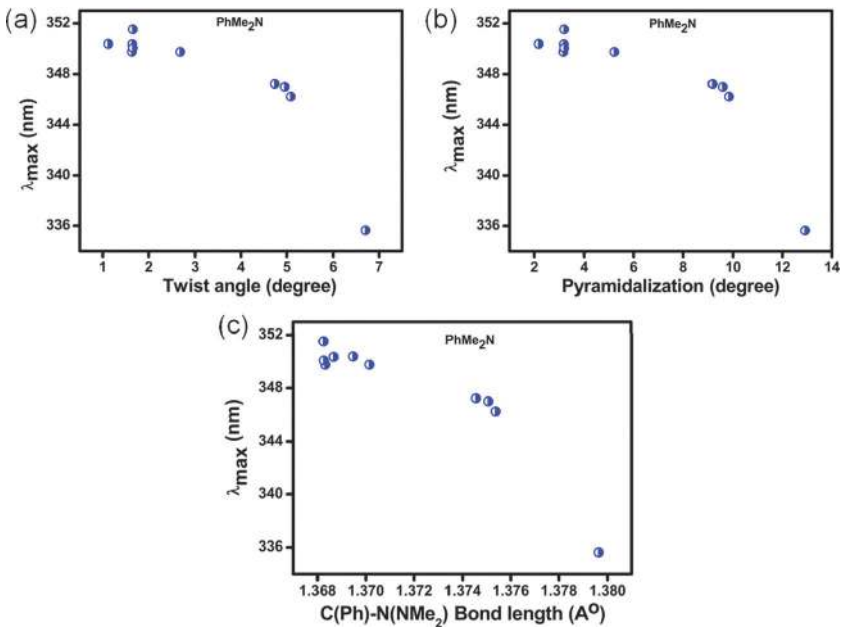

Fig. 8 Correlation between vertical excitation energy and (a) twist angle of NMe_2, (b) pyramidalization of NMe_2, and (c) C(Ph)–N(NMe_2) bond length in **$PhMe_2N$**.

ESI† for others). It is observed that higher the twist angle, and pyramidalization of the NMe_2 group, higher is the excitation energy of the NMe_2 containing derivative (Fig. 8a and b). Vertical excitation energy is also found to be higher for the case of the longer C(Ph)–N(NMe_2) bond length (Fig. 8c). The data indicate that better the planarity of the NMe_2 group with the phenyl ring, better is the delocalization of electrons from the NMe_2 group to the phenyl ring (see Fig S3, ESI† for Mulliken charge analysis), and thus smaller is the excitation energy.

Correlation of solvent polarity with ground state oscillator strength and dipole moment

From Fig. 9a, the change in oscillator strength with the dielectric constant has been noted to be interesting. There is considerable enhancement of oscillator strength on moving from gas phase to non-polar solvents like heptane and cyclohexane. The oscillator strength decreases from non-polar cyclohexane to polar methanol with a slight increase of oscillator strength for CH_3CN, and DMF. On the other hand, the dipole moment is found to increase with increasing dielectric constant (Fig. 9b). Similar to oscillator strength, the dipole moment is also observed to increase from the gas phase to heptane and cyclohexane. The donor–acceptor derivative **Me_2NCN** exhibits the highest dipole moment. It is important to note that the derivative **PhCN** having one strong electron withdrawing CN group possesses a higher dipole moment than **$PhMe_2$N** which has a strong electron donating NMe_2 group. Anticipatorily, the derivatives **Me_2NMe_2N** having two strong electron withdrawing NMe_2 groups and the neutral derivative **PhPh** are found to have the lowest dipole moment.

Excited state geometry and the effect of solvent

The excited state geometry calculation was started with two stationary geometries at the first excited state. One of the excited state geometries, which is planar (see Fig. S20, ESI†), was obtained from the optimized ground state geometry. On the other hand, another excited state geometry was achieved through 90° rotation of the two phenyl rings around the butadiyne moiety in optimized ground state geometry. The planar geometry leads to a LE state emission while the second geometry promotes to an ICT emission. Out of the three donor–donor derivatives **OMeOMe**, **Me_2NOMe**, and **Me_2NMe_2N**, the derivative **Me_2NOMe** has been chosen here to study the geometry of the ICT emissive state along with **PhOMe**, **$PhMe_2$N**, **PhCN**, and **Me_2NCN**.

At this point, the ICT geometry attracts special attention owing to the fact that the two phenyl rings are twisted and almost perpendicular to each other. To our surprise, in addition to perpendicular geometry of the ICT state, a bending of the butadiyne moiety has been observed for the derivatives **$PhMe_2$N**, **PhOMe**, and **Me_2NOMe** (Fig. 10a–c). On the other hand, no bending of the butadiyne moiety has been noted for the fluorophores **PhCN** and **Me_2NCN** (Fig. 10d and e). The important point is to note that the butadiynyl derivatives irrespective of the peripheral electronic substitutions are prone to the twisting conformation around the butadiyne moiety in the ICT emissive state. Our earlier experimental findings on the photophysics of butadiynyl derivatives revealed the strong intramolecular charge transfer character of such derivatives.[16] Thus, this theoretical finding of the twisted conformation of the ICT state probably indicates twisted intramolecular charge transfer (TICT) behaviour for the butadiynyl derivatives. At this juncture, it is worth stressing that while the TICT behavior, which is common in NMe_2 or NEt_2 containing donor–acceptor fluorophores, actually means the twisting of dialkyl substituted amine moiety with respect to the attached planar aromatic moiety, here, for the butadiynyl derivatives, it means the twisting of one phenyl ring with respect to the another phenyl ring around the butadiyne bridge. Even the derivatives **$PhMe_2$N**, **Me_2NOMe**, and **Me_2NCN** where the NMe_2 group is present bear the NMe_2 group almost in the same plane with the attached phenyl ring in the ICT emissive state. Thus, if the dialkyl amine substituted phenyl ring is conjugated through

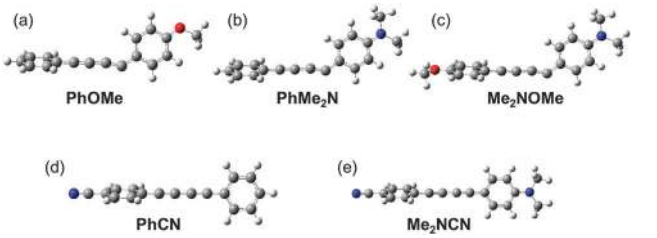

Fig. 10 Optimized geometry of (a) **PhOMe**, (b) **$PhMe_2$N**, (c) **Me_2NOMe**, (d) **PhCN**, and (e) **Me_2NCN** in the ICT emissive state in CH_3CN using B3LYP/6-311G(d,p) level of theory.

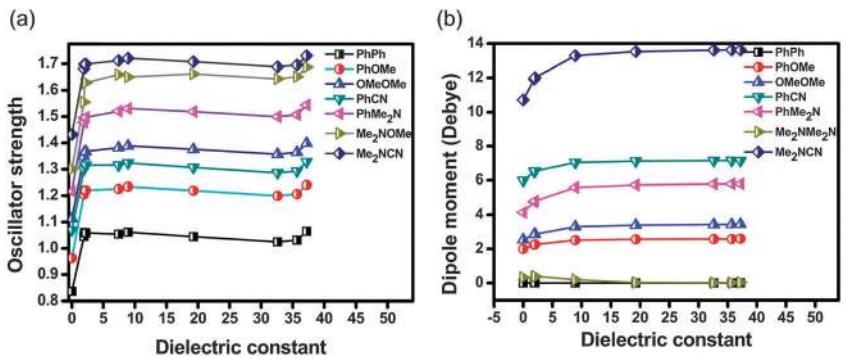

Fig. 9 Variation of (a) oscillator strength (CAM-B3LYP/6-311+G(d,p)) and (b) dipole moment (B3LYP/6-311G(d,p)) with the dielectric constant.

Table 4 C(Ph)–N(NMe_2) and C(Ph)–O(OMe) bond length in the excited state

	Ground state		Excited state			
			Planar		Twisted	
Bond length (Å)	Cyclo[a]	CH_3CN	Cyclo	CH_3CN	Cyclo	CH_3CN
C(Ph)–N(NMe_2) bond length in **$PhMe_2N$**	1.375	1.368	1.368	1.363	1.357	1.340
C(Ph)–O(OMe) bond length in **PhOMe**	1.357	1.355	1.352	1.345	1.337	1.331

[a] Cyclo indicates cyclohexane.

the butadiyne bridge with another phenyl ring it is likely that the twisting in the ICT state will occur between the two aromatic rings along the butadiyne conjugation and twisting of such derivatives will not necessarily mean the twist of the amine group.

At this stage, we were particularly keen to look at the C(Ph)–N(NMe_2) bond length of the derivatives in cyclohexane and CH_3CN. The fluorophore **$PhMe_2N$** was chosen here as the representative. Table 4 demonstrates that the C(Ph)–N(NMe_2) bond length decreases from the planar to twisted geometry in cyclohexane and CH_3CN respectively. The decrease of the bond length could be attributed to the charge transfer character of the twisted ICT state. A similar observation was also found for the C(Ph)–O(OMe) bond length in **PhOMe** where the C(Ph)–O(OMe) bond length is observed to decrease from planar to twisted geometry in the excited state (Table 4).

LE and ICT emission energies

In an effort to evaluate LE and ICT emission energies of the butadiynyl fluorophores, a series of DFT functionals such as B3LYP, PBE0, M052X, LC-BLYP, and CAM-B3LYP were tested. The 6-311+G(d,p) basis set was considered for fluorescence energy calculation without further screening of the basis set. It is observed from Table 5 that the B3LYP functional yields a better result for LE emission compared with the experimental values. On the other hand, the CAM-B3LYP functional produces good results for ICT emission energies which are closer to experimental values (Table 6).

At this juncture, considering the possibility of charge transfer related problems being embedded in the TD-B3LYP optimized ICT geometry, the ICT geometry of the **$PhMe_2N$** was optimized with TD-CAM-B3LYP as a test study and thus, the obtained geometry was used for the vertical de-excitation

Table 5 LE emission energy using different functionals and the 6-311+G(d,p) basis set

	LE emission energies (in eV) in CH_3CN					
Molecules	Expt.[a]	B3LYP	PBE0	M052X	LC-BLYP	CAM-B3LYP
PhOMe	2.93	2.94	3.01	3.21	3.30	3.13
$PhMe_2N$	2.64	2.80	2.87	3.12	3.28	3.07

[a] Ref. 16.

Table 6 ICT emission energy using different functionals and the 6-311+G(d,p) basis set

	ICT emission energies (in eV) in CH_3CN					
Molecules	Expt.[a]	B3LYP	PBE0	M052X	LC-BLYP	CAM-B3LYP
PhOMe	2.45	2.13	2.19	2.11	2.37	2.31
$PhMe_2N$	2.20	1.91	1.99	2.05	2.38	2.23

[a] Ref. 16.

energy calculation. The calculated emission energy (2.10 eV) using the TD-CAM-B3LYP optimized geometry was in reasonably good agreement with the experimental one (2.20 eV). However it did not produce any better result than the result obtained from the previous methodology (2.23 eV). The difference of 0.13 eV emission energy calculated from B3LYP and CAM-B3LYP optimized ICT geometry could be attributed to the minor geometrical changes of the two optimized geometries (see Fig. S21, ESI†).

It is evident from Tables 5 and 6 that although the CAM-B3LYP functional substitutes other functionals in predicting charge transfer energies of the butadiynyl fluorophores, the B3LYP functional takes credit in calculating LE emission energies of the derivatives. Again, to our surprise, ICT emission energies of the derivatives **PhCN**, and **Me_2NCN**, where the two phenyl rings are perpendicular but the butadiyne moiety is not bent, were found to be accurate using the B3LYP functional rather than the CAM-B3LYP functional (see Table S3, ESI†). Thus, it is noted that the accuracy of the functionals is much better for calculating absorption energies rather than calculating emission energies, which is again not surprising. However, at this juncture, the success of the B3LYP functional over the CAM-B3LYP functional in predicting LE emission energy needs to be addressed. In the earlier section where vertical absorption energies and molecular orbitals were discussed, it has been mentioned that the charge transfer absorption mainly involves the HOMO to the LUMO for the $S_0 \rightarrow S_1$ state. This observation for the butadiynyl fluorophores

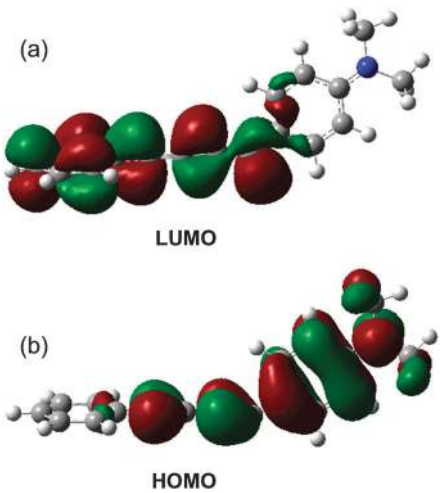

Fig. 11 (a) HOMO and (b) LUMO of **$PhMe_2N$** in the ICT emissive state in CH_3CN.

has been found to be the same in all the calculations invoking different functionals. However, the B3LYP functional exhibits a minor contribution for the $S_0 \rightarrow S_1$ transition in addition to the major contribution of HOMO to LUMO transition. It is the minor contribution which actually contributes to the LE state, which has been mentioned in our earlier article.[16] Thus, here, in our excited state study, the success of the B3LYP functional in predicting LE emission energies is although not surprising, attracts special attention.

Molecular orbitals and intramolecular charge transfer

Fig. 11 demonstrates that the HOMO of the ICT emissive state of **PhMe$_2$N** mainly constitutes the donor moiety—the dimethylamino group substituted phenyl ring and the butadiyne moiety. On the other side, the LUMO of the ICT state of **PhMe$_2$N** spreads over the acceptor moiety—the unsubstituted phenyl ring and the butadiyne moiety. Such localization of HOMO and LUMO electron density on donor and acceptor parts of the fluorophore respectively is attributed to the strong ICT character of the fluorophore (see Fig. S22, ESI† for HOMO and LUMO for other fluorophores). The noteworthy observation is that the butadiyne moiety acts as a bridge between the donor and acceptor moieties assisting the system in the ICT process. In our earlier work,[16] we hinted this ICT character of the butadiynyl fluorophores through ground state molecular orbital calculations. In this article, the aforementioned observation of electronic distributions in molecular orbitals being in the excited state unambiguously supports the ICT behaviour of the butadiynyl fluorophores. Moreover, the red shifted emission (Table 6) originating from the twisted geometry compared to that of the planar geometry (Table 5) assures the ICT emission.

Absorption and emission transition dipole moment vectors

Comprehending the absorption and emission characteristics of the fluorophores, at the end, our attention was directed at the understanding of transition dipole moment (TDM) vectors of the fluorophores. The absorption TDM vector of the fluorophores (Fig. 12), which have a strong donor NMe_2 group, lies along the long axis of the fluorophores and pointing away from the donor part. Such observation, that is, orientation of the TDM vector along the long axis is also noted for the derivatives which contain a strong acceptor CN group such as **PhCN** and **Me$_2$NCN**. For the derivatives **PhCN** and **Me$_2$NCN**, the TDM vector originates from the unsubstituted phenyl ring which is the donor part of the fluorophores. Interestingly, the fluorophores which have the OMe group as a weak electron donor have the TDM vector along the short axis of the molecules. For example, the fluorophore **OMeOMe** which has two weak

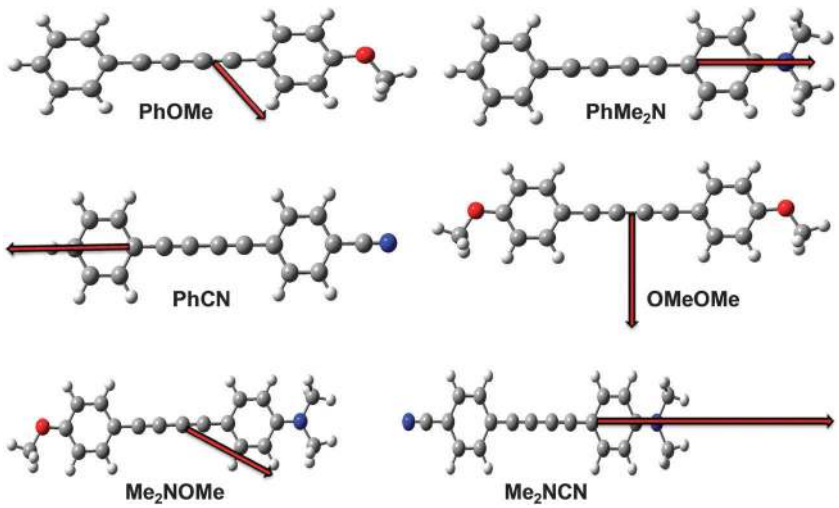

Fig. 12 Absorption transition dipole moment in CH_3CN using CAM-B3LYP/6-311+G(d,p) level of theory.

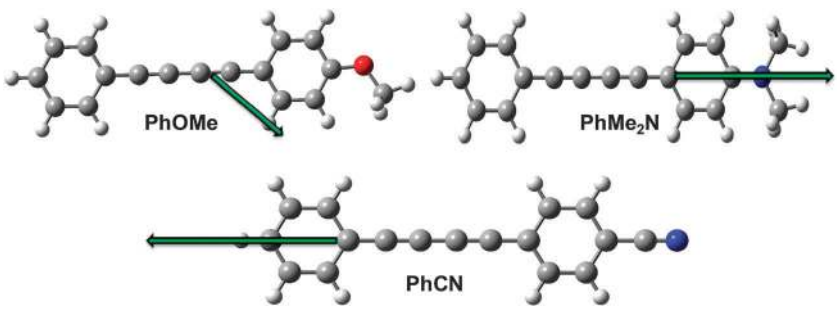

Fig. 13 LE transition dipole moment in CH_3CN using CAM-B3LYP/6-311+G(d,p) level of theory.

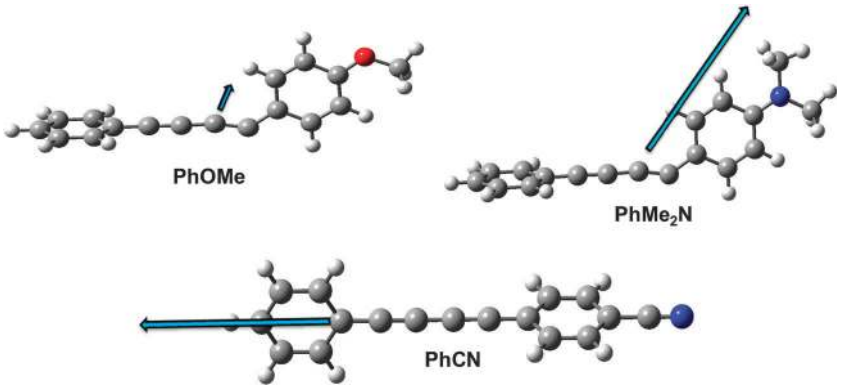

Fig. 14 ICT transition dipole moment in CH_3CN using CAM-B3LYP/6-311+G(d,p) level of theory.

donating OMe groups possesses the TDM vector almost parallel to the short molecular axis of the derivative. The TDM vector of the molecule **PhOMe** which has only one weak donor OMe group makes an angle with the long molecular axis of the derivative. Even the angle approaches closer to the long molecular axis for the derivative **Me_2NOMe** which contains a weak donor OMe and a strong donor NMe_2 group. Thus, the absorption TDM vectors of the butadiynyl fluorophores are found to orient either along the short axis or the long axis depending on the nature of the substituent present at the periphery of the diphenyl butadiyne moiety.

The TDM vector for the LE emission (Fig. 13) was found to be almost in a similar direction like absorption TDM. But, the magnitude of TDM for LE emission differs from the absorption TDM (see Table S4, ESI† for TDM values). The TDM vector for ICT emission (Fig. 14) is very interesting. For the fluorophores which have the NMe_2 group such as **PhMe_2N**, the TDM vector shifts its position from the long axis to the short axis unlike absorption TDM and LE TDM (Fig. 14).

Conclusion

In conclusion, a detailed theoretical investigation of the geometry of ground and excited states, absorption and fluorescence properties of a series of diphenyl butadiynyl fluorophores through the assessment of several TDDFT functionals with the inclusion of solvent effects has been accomplished. The very important outcomes of the present investigation can be summarized as follows:

(1) CAM-B3LYP functional was found to be very accurate in the calculation of charge transfer electronic absorption energies of the butadiynyl fluorophores. CAM-B3LYP functional was also found to give good results for ICT emission energies while B3LYP was found to be effective for the calculation of LE emission energies. On the other hand, hybrid functionals such as B3LYP and PBE0 were observed to produce TDDFT PES with the good description of the stability of LE and ICT states as a function of torsional angle.

(2) The intramolecular charge transfer emission of the fluorophores was observed to originate from the TICT state where the two phenyl rings are found to be perpendicular to each other around the butadiyne bridge. The bending of the butadiyne moiety for the donor–donor and donor–neutral substituted phenyl ring containing butadiynyl fluorophores in the ICT emissive state is noteworthy owing to the fact that bending of the butadiyne moiety is not trivial in the solution state.

(3) The orientation of the transition dipole moment (TDM) vector of the butadiynyl fluorophores was found to be different for the fluorophores. Although the core backbone moiety of all the fluorophores is the same that is diphenyl butadiyne, it is the substituent at the periphery of the diphenyl butadiyne which strongly directs the direction of the TDM vector.

Thus, we believe that our studies usher in a new platform to understand and analyze the absorption and emission properties of the butadiynyl fluorophores and thus will help in prior designing of new synthetic advanced butadiynyl fluorophores minimizing synthetic efforts and costs.

Acknowledgements

The authors thank DST, New Delhi, for financial support. High performance computing facility of IIT Madras is greatly acknowledged. AKP thanks CSIR, New Delhi, for research fellowship.

References

1 S. T. Wu, H. H. B. Meng and L. R. Dalton, *J. Appl. Phys.*, 1991, **70**, 3013–3017.
2 S. T. Wu, J. D. Margerum, H. B. Meng, L. R. Dalton, C. S. Hsu and S. H. Lung, *Appl. Phys. Lett.*, 1992, **61**, 630–632.
3 S.-T. Wu, M. E. Neubert, S. S. Keast, D. G. Abdallah, S. N. Lee, M. E. Walsh and T. A. Dorschner, *Appl. Phys. Lett.*, 2000, **77**, 957–959.
4 M. F. Beristain, T. Ogawa, G. Gomez-Sosa, E. Muñoz, Y. Maekawa, F. Halim, F. Smith, A. Walser and R. Dorsinville, *Mol. Cryst. Liq. Cryst.*, 2010, **521**, 237–245.
5 G. S. Kottas, L. I. Clarke, D. Horinek and J. Michl, *Chem. Rev.*, 2005, **105**, 1281–1376.
6 T. J. Taylor and F. P. Gabbaï, *Organometallics*, 2006, **25**, 2143–2147.

7 O. Sari, V. Roy, J. Balzarini, R. Snoeck, G. Andrei and L. A. Agrofoglio, *Eur. J. Med. Chem.*, 2012, **53**, 220–228.
8 P. W. Thulstrup, S. V. Hoffmann, B. K. V. Hansen and J. Spanget-Larsen, *Phys. Chem. Chem. Phys.*, 2011, **13**, 16168–16174.
9 T. Hoshi, J. Okubo, M. Kobayashi and Y. Tanizaki, *J. Am. Chem. Soc.*, 1986, **108**, 3867–3872.
10 T. Takabe, M. Tanaka and J. Tanaka, *Bull. Chem. Soc. Jpn.*, 1974, **47**, 1912–1916.
11 M. Kijima, I. Kinoshita and H. Shirakawa, *J. Mol. Struct.*, 2000, **521**, 279–283.
12 G. Baranović, L. Colombo, K. Furić, J. R. Durig, J. F. Sullivan and J. Mink, *J. Mol. Struct.*, 1986, **144**, 53–69.
13 B. Zimmermann and G. Baranović, *Vib. Spectrosc.*, 2006, **41**, 126–135.
14 R. A. Nyquist and C. L. Putzig, *Vib. Spectrosc.*, 1992, **4**, 35–38.
15 A. N. Swinburne, M. J. Paterson, A. Beeby and J. W. Steed, *Chem. – Eur. J.*, 2010, **16**, 2714–2718.
16 A. K. Pati, M. Mohapatra, P. Ghosh, S. J. Gharpure and A. K. Mishra, *J. Phys. Chem. A*, 2013, **117**, 6548–6560.
17 X. Ma, L. Yan, X. Wang, Q. Guo and A. Xia, *Phys. Chem. Chem. Phys.*, 2011, **13**, 17273–17283.
18 Y. Nagano, T. Ikoma, K. Akiyama and S. Tero-Kubota, *J. Am. Chem. Soc.*, 2003, **125**, 14103–14112.
19 A. D. Becke, *J. Chem. Phys.*, 1993, **98**, 1372–1377.
20 A. D. Becke, *J. Chem. Phys.*, 1993, **98**, 5648–5652.
21 A. D. Boese and J. M. L. Martin, *J. Chem. Phys.*, 2004, **121**, 3405–3416.
22 Y. Zhao and D. G. Truhlar, *Acc. Chem. Res.*, 2008, **41**, 157–167.
23 Y. Zhao and D. Truhlar, *Theor. Chem. Acc.*, 2008, **120**, 215–241.
24 R. E. Stratmann, G. E. Scuseria and M. J. Frisch, *J. Chem. Phys.*, 1998, **109**, 8218–8224.
25 E. Runge and E. K. U. Gross, *Phys. Rev. Lett.*, 1984, **52**, 997–1000.
26 A. Dreuw and M. Head-Gordon, *Chem. Rev.*, 2005, **105**, 4009–4037.
27 D. Jacquemin, B. Mennucci and C. Adamo, *Phys. Chem. Chem. Phys.*, 2011, **13**, 16987–16998.
28 M. E. Casida, *THEOCHEM*, 2009, **914**, 3–18.
29 D. J. Tozer, *J. Chem. Phys.*, 2003, **119**, 12697–12699.
30 A. Dreuw and M. Head-Gordon, *J. Am. Chem. Soc.*, 2004, **126**, 4007–4016.
31 A. Dreuw, J. L. Weisman and M. Head-Gordon, *J. Chem. Phys.*, 2003, **119**, 2943–2946.
32 M. E. Casida, F. Gutierrez, J. Guan, F.-X. Gadea, D. Salahub and J.-P. Daudey, *J. Chem. Phys.*, 2000, **113**, 7062–7071.
33 Y. Tawada, T. Tsuneda, S. Yanagisawa, T. Yanai and K. Hirao, *J. Chem. Phys.*, 2004, **120**, 8425–8433.
34 C. Jamorski, J. B. Foresman, C. Thilgen and H.-P. Lüthi, *J. Chem. Phys.*, 2002, **116**, 8761–8771.
35 N. T. Maitra, *J. Chem. Phys.*, 2005, **122**, 234104.
36 O. Gritsenko and E. J. Baerends, *J. Chem. Phys.*, 2004, **121**, 655–660.
37 P. M. W. Gill, R. D. Adamson and J. A. Pople, *Mol. Phys.*, 1996, **88**, 1005–1009.
38 T. Leininger, H. Stoll, H.-J. Werner and A. Savin, *Chem. Phys. Lett.*, 1997, **275**, 151–160.
39 H. Iikura, T. Tsuneda, T. Yanai and K. Hirao, *J. Chem. Phys.*, 2001, **115**, 3540–3544.
40 J. Heyd, G. E. Scuseria and M. Ernzerhof, *J. Chem. Phys.*, 2003, **118**, 8207–8215.
41 J. Toulouse, F. Colonna and A. Savin, *Phys. Rev. A: At., Mol., Opt. Phys.*, 2004, **70**, 062505.
42 T. Yanai, D. P. Tew and N. C. Handy, *Chem. Phys. Lett.*, 2004, **393**, 51–57.
43 E. Rudberg, P. Sałek, T. Helgaker and H. Ågren, *J. Chem. Phys.*, 2005, **123**, 184108.
44 M. Kamiya, H. Sekino, T. Tsuneda and K. Hirao, *J. Chem. Phys.*, 2005, **122**, 234111.
45 T. Yanai, R. J. Harrison and N. C. Handy, *Mol. Phys.*, 2005, **103**, 413–424.
46 Z.-L. Cai, M. J. Crossley, J. R. Reimers, R. Kobayashi and R. D. Amos, *J. Phys. Chem. B*, 2006, **110**, 15624–15632.
47 M. J. G. Peach, T. Helgaker, P. Salek, T. W. Keal, O. B. Lutnaes, D. J. Tozer and N. C. Handy, *Phys. Chem. Chem. Phys.*, 2006, **8**, 558–562.
48 M. Chiba, T. Tsuneda and K. Hirao, *J. Chem. Phys.*, 2006, **124**, 144106.
49 O. A. Vydrov and G. E. Scuseria, *J. Chem. Phys.*, 2006, **125**, 234109.
50 O. A. Vydrov, J. Heyd, A. V. Krukau and G. E. Scuseria, *J. Chem. Phys.*, 2006, **125**, 074106.
51 T. M. Henderson, A. F. Izmaylov, G. E. Scuseria and A. Savin, *J. Chem. Phys.*, 2007, **127**, 221103.
52 T. M. Henderson, B. G. Janesko and G. E. Scuseria, *J. Chem. Phys.*, 2008, **128**, 194105.
53 M. J. G. Peach, P. Benfield, T. Helgaker and D. J. Tozer, *J. Chem. Phys.*, 2008, **128**, 044118.
54 M. J. Frisch, *et al., Gaussian 09, Revision C.01*, Gaussian, Inc., Wallingford, CT, 2010.
55 A. D. Becke, *Phys. Rev. A: At., Mol., Opt. Phys.*, 1988, **38**, 3098–3100.
56 C. Lee, W. Yang and R. G. Parr, *Phys. Rev. B: Condens. Matter Mater. Phys.*, 1988, **37**, 785–789.
57 J. P. Perdew, K. Burke and M. Ernzerhof, *Phys. Rev. Lett.*, 1996, **77**, 3865–3868.
58 C. Adamo and V. Barone, *J. Chem. Phys.*, 1999, **110**, 6158–6170.
59 M. Ernzerhof and G. E. Scuseria, *J. Chem. Phys.*, 1999, **110**, 5029–5036.
60 Y. Zhao, N. E. Schultz and D. G. Truhlar, *J. Chem. Theory Comput.*, 2006, **2**, 364–382.
61 J.-W. Song, T. Hirosawa, T. Tsuneda and K. Hirao, *J. Chem. Phys.*, 2007, **126**, 154105.
62 H. L. Schmider and A. D. Becke, *J. Chem. Phys.*, 1998, **108**, 9624–9631.
63 J. Tomasi, B. Mennucci and R. Cammi, *Chem. Rev.*, 2005, **105**, 2999–3093.

